

NUMERICAL STUDY ON HEAT AND FLOW TRANSFER CHARACTERISTICS IN RECTANGULAR MINI-CHANNEL WITH S-SHAPED TURBULATOR INSERTED

by

Yongqiang FANG, Fanmao MENG*, Yinhang XI, and Anchao ZHANG

School of Mechanical and Power Engineering, Henan Polytechnic University, Jiaozuo, China

Original scientific paper

<https://doi.org/10.2298/TSCI220919210F>

The mini-channel heat exchanger has better heat and flow transfer characteristics than conventional heat exchanger. In this study, we use the S-shaped turbulator inserted, which is simple to install and inexpensive, to improve the heat exchange. The fluid-flow and heat transfer characteristics in smooth and inserted S-shaped turbulator rectangular mini-channels are simulated by numerical simulation under constant wall temperature heating in the Reynolds number 198.77-1987.67. The results of the numerical simulation show that compared with the smooth mini-channel, the pressure drop of the three rectangular mini-channels with different inserted S-shaped turbulators with radii on the horizontal axis of 1 mm, 1.5 mm, and 2 mm increase by 334.8-774.3%, 275.9-606.4%, and 234.6-500.4%. The average Nusselt numbers grow by 28.7-98.6%, 18.8-92% and 11.1-88.5%. The total thermal resistances reduce by 22.43-50.15%, 15.91-48.40%, and 10.08%-47.45%. The field coordination numbers increase by 30.36%-115.29%, 19.72-106.94%, and 19.72-104.72%. Moreover, the non-linear regression method establishes the prediction formulas of the pressure drop and average Nusselt number. In most cases, the deviation between the predicted and simulated values is between $\pm 4.6\%$ and $\pm 14\%$.

Key words: mini-channel, S-shaped turbulator, heat transfer, laminar flow, CFD

Introduction

The utilization of energy is often inseparable from the transfer of heat. Scientists have done a lot of research on the influence of various structures of heat exchangers on heat transfer and flow characteristics. With the development of technology, regular size channel heat exchangers can no longer meet the heat transfer requirements in some cases. Tuckerman and Pease [1] first proposed the concept of micro-channels and found that the heat flux density of micro-channel heat exchangers can reach 790 W/cm^2 . Lelea *et al.* [2]. Shah and London [3], and Blevins [4] theoretically studied the mini/micro-channel and demonstrated the applicability of the Navier-Stokes equation it. The methods used to enhance heat exchange in mini/micro-channels are mainly active reinforcement or passive reinforcement. Active reinforcement has certain limitations [5-10]. Passive reinforcement is widely used because of its easy installation, convenient maintenance and low cost. Standard passive reinforcements include channel shape changes, inserts, nanofluidics [11].

Qu and Mudawar [12] showed that when the Reynolds number is 139-1672, the smooth mini/micro-channel is in the laminar flow stage and does not transition turbulent flow in advance. Moreover, the smooth mini/micro-channel laminar flow research approach is appropriate. Tian

* Corresponding author, e-mail: hpumfm@163.com

et al. [13] and Sohankar [14] suggested that fins, spoiler columns and ribs in mini/micro-channels can generate vortices to increase heat exchange. Wang *et al.* [15] used a numerical method to study the effect of discrete double diagonal ribs on the heat transfer and flow performance of rectangular micro-channels. Fiebig [16] and Ebrahimi [17] thought rectangular mini/micro-channels with varied fins have better heat transfer performance than smooth channels. Datta *et al.* [18] investigated the effect of the fin angle on mini/micro-channels. They claimed that when the Reynolds number exceeds 600, the 30° rectangular fin angle has the highest overall performance. Yadav *et al.* [19] and Jia *et al.* [20] demonstrated that increasing the pin-fin diameter and height would strengthen the heat exchange of the micro-channel. The Nusselt number of the mini-channel grows as the twist rate of the built-in twist band decreases and the twist length increases, according to Feng *et al.* [21]. Kurnia *et al.* [22] verified the vortex structure through particle image velocimetry experiments. Sroysroy and Eiamsard [23] found that the square cut twisted tape inserted in the tube has a 36-45% higher Nusselt number and a 19-29% lower frictional resistance than the traditional twisted tape. Zheng *et al.* [24] argued that the longitudinal vortex generator (LVG) with trapezoidal cross-sections is beneficial for enhancing heat exchange and improving the overall performance of micro-channel heat sinks. Through numerical studies, Ebrahimi and Naranjani [25] indicated that the overall heat transfer efficiency of the conical protruding channel was 12.0-169.4% higher than that of the smooth channel. The heat exchange performance of the rectangular channel of LVG in the laminar flow region increased with the Reynolds number [26]. Sui *et al.* [27] indicated that between $Re = 300-800$, the heat exchange performance of the wave-form micro-channel is higher than that of the straight baseline micro-channel. The pressure drop is much smaller than that of the straight micro-channel. Zhu *et al.* [28] found that micro-channels with trapezoidal grooves have good heat transfer performance. Lin *et al.* [29] studied the heat transfer performance of a new curved trapezoidal vortex generator stamping fin.

Inner-insert enhanced heat exchange technology is widely used in passive enhanced heat exchange technology. Turbulators have become the focus of the research on inner-insert enhanced heat exchange technology due to their easy manufacture, low cost and anti-scaling solid ability. However, the mini-channel with an *S*-shaped turbulator inserted has rarely been studied. Therefore, this paper chooses to study the enhanced heat transfer of mini-channels with an *S*-shaped turbulator inserted. The impact of different structural parameters of *S*-shaped

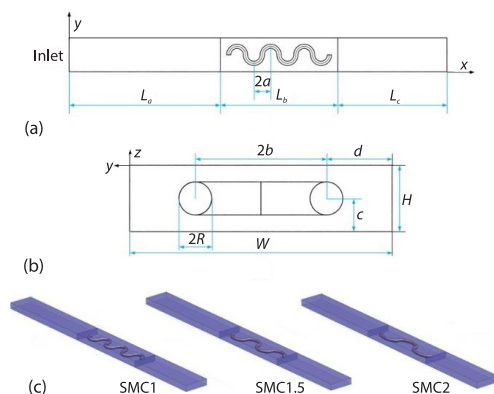


Figure 1. The geometric details of the rectangular mini-channel with an *S*-shaped turbulator inserted (a) top view, (b) side view, and (c) 3-D view of three different transverse axis radius

turbulators on the laminar flow and heat exchange properties of rectangular mini-channels was studied by numerical simulation. Through non-linear regression analysis, the correlation of the Average Nusselt number of the rectangular mini-channel with an *S*-shaped turbulator inserted is summarized, which is used to provide a prediction method for the general situation.

Thermodynamic analysis

Figure 1 shows the geometric details of the mini-channel inserted into the *S*-shaped turbulator. Figure 1(a) is a top view, the length of the inlet section is L_a , the length of the heating section is L_b , and the length of the outlet section is L_c . Figure 1(b) is a side view, the height of the rectangular mini-channels is H and the

width is W . The S -shape turbulator is inserted in the heating section. The distances between the S -shaped turbulator and the channel wall are c and d , respectively. The S -shaped turbulator is made by bending metal wire. The wire is bent into an S -shape. It has a radius of R . Its vertical axis radius is b and its horizontal axis radius is a . Figure 1(c) is a 3-D image of the three rectangular mini-channels with different horizontal axis radii S -shaped turbulators. From left to right, SMC1, SMC1.5, and SMC2 (the smooth rectangular mini-channel is denoted as SMC) are shown in fig. 1(c). The SMC1 is a rectangular mini-channel with an S -shaped turbulator of a horizontal axis radius of 1 mm. The SMC1.5 is a rectangular mini-channel with an S -shaped turbulator of a horizontal axis radius of 1.5 mm. The SMC2 is a rectangular mini-channel with an S -shaped turbulator of a horizontal axis radius of 2 mm. Table 1 is the geometric parameter table of rectangular mini-channels with different S -shaped turbulators.

Table 1. The geometric parameter table of the rectangular mini-channels with different S -shaped turbulators

Channel type	a [mm]	b [mm]	c [mm]	d [mm]	L_a [mm]	L_b [mm]	L_c [mm]
SMC	–	–	–	–	18	13	14
SMC1	1	1	0.5	1	18	13	14
SMC1.5	1	1.5	0.5	1	18	13	14
SMC2	1	2	0.5	1	18	13	14

The material of the mini-channel walls and turbulators in the simulation is aluminum and the fluid is water. To simplify the calculation, make the following assumptions:

- The fluid is incompressible and Newtonian fluid. The fluid-flow is in a 3-D steady laminar state.
- Gravity and other body forces are ignored. The effects of radiative heat transfer and viscous dissipation are ignored.
- The fluid has fully developed when it enters the heating section. No-slip boundary conditions are specified on both the channel walls and the solid-fluid interface.
- The dynamic viscosity and thermal conductivity of the fluid are related to its temperature and are variable physical parameters, while other physical parameters remain unchanged. The physical properties of solids are constant.

Based on the previous assumptions, the control equations of the fluid region are established as follows. Continuity equation is eq. (1). Where U fluid is the velocity vector and ρ_f is the fluid density:

$$\nabla(\rho_f U) = 0 \tag{1}$$

Momentum equation is eq. (2) where μ_f is the fluid dynamic viscosity and P – the fluid pressure:

$$\nabla(\rho_f U U) = -\nabla P + \nabla(\mu_f \nabla U) \tag{2}$$

where $c_{p,f}$ is the specific heat of the fluid, T_f – the temperature of the fluid, and λ_f – the thermal conductivity of the fluid. Energy equation:

$$\nabla(\rho_f c_{p,f} U T_f) = \nabla(\lambda_f \nabla T_f) \tag{3}$$

Hydraulic diameter:

$$D_h = \frac{4A_c}{P} \tag{4}$$

Reynolds number:

$$\text{Re} = \frac{\rho_f u_{\text{in}} D_h}{\mu_f} \quad (5)$$

Inlet and outlet pressure drop:

$$\Delta P = P_{\text{in}} - P_{\text{out}} \quad (6)$$

The temperature difference between the heating surface and the fluid is the logarithmic temperature difference and can be written:

$$\Delta T = \frac{T_{\text{out}} - T_{\text{in}}}{\ln \frac{T_{\text{wall}} - T_{\text{in}}}{T_{\text{wall}} - T_{\text{out}}}} \quad (7)$$

where A is the heating surface area and Q – the heat exchange. Average convective heat transfer coefficient:

$$h_{\text{ave}} = \frac{Q}{A \Delta T_m} \quad (8)$$

local convective heat transfer coefficient:

$$h_x = \frac{Q}{A(T_{w,x} - T_{f,x})} \quad (9)$$

Total thermal resistance:

$$R_T = \frac{\Delta T_m}{Q} \quad (10)$$

where λ_f fluid thermal conductivity. Average Nusselt number:

$$\text{Nu}_{\text{ave}} = \frac{h_{\text{ave}} D_h}{\lambda_f} \quad (11)$$

Local Nusselt number:

$$\text{Nu}_x = \frac{h_x D_h}{\lambda_x} \quad (12)$$

Dimensionless distance:

$$x^* = \frac{x}{D_h \text{Re} \text{Pr}} \quad (13)$$

where β is the synergy angle between the fluid velocity vector and the pressure gradient. The synergistic relationship between the fluid velocity vector and pressure gradient is eq. (13):

$$U \nabla P = |U| |\nabla P| \cos \beta \quad (14)$$

where α is the synergy angle between the fluid velocity vector and the temperature gradient. The synergistic relationship between the fluid velocity vector and temperature gradient is eq. (14):

$$U \nabla T = |U| |\nabla T| \cos \alpha \quad (15)$$

Field co-ordination number is eq. (15).

$$Fc = \int (U \nabla T) dy = \frac{Nu_{ave}}{Re Pr} \quad (16)$$

Prandtl number:

$$Pr = \frac{c_{p,f} \mu_f}{\lambda_f} \quad (17)$$

In this paper, the CFD simulation method is used to discretize the continuous, momentum and energy conservation equations based on boundary conditions using the finite volume method. Structured meshes of solid and fluid regions were generated using GAMBIT 2.4.6 and the meshes were validated. The ANSYS FLUENT was used to solve the governing equations for the heat transfer and flow performance of the rectangular mini-channel with an S-shaped turbulator inserted. Coupling of velocity and pressure equations by SIMPLEC algorithm. The second-order upwind form is used to spatially discretize the convection and diffusion elements of the momentum equation. The convergence criterion is when the normalized residuals for all variables in the continuity, momentum and energy equations are less than 10^{-6} . Detailed boundary condition settings are shown in tab. 2.

Table 2. Boundary condition

Boundary	Setting
Inlet	$u = 0.1 \sim 1 \text{ m/s}, T_{in} = 303.15 \text{ K}$
Outlet	Free outflow
Four side walls of heating section	Constant wall temperature and $T_w = 333.15 \text{ K}$
Four side walls of inlet and outlet section	Non-slip adiabatic boundary
S-shaped turbulators	Non-slip adiabatic boundary

Four different grids are studied to verify the grid independence. The four grid numbers are 320000, 420000, 470000, and 570000, respectively. The average Nusselt number and pressure drop of the four grids are shown in fig. 2(a). The average Nusselt number and pressure drop difference between the 420000 and 470000 grids are 0.08% and 0.04%, respectively. The relative differences in the average Nusselt number and pressure drop for the 470000 and 570000 grids are 0.05% and 0.07%, respectively. Therefore, the 470000 grid element number is

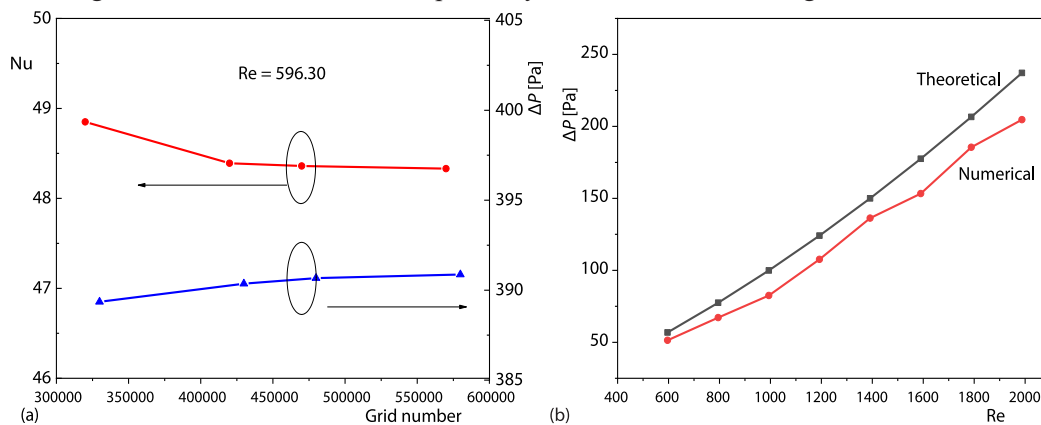


Figure 2. (a) Variation of grid independence and (b) theoretical verification

selected as the reference grid size. To ensure the accuracy of numerical simulation results, the pressure drop simulation results of smooth straight pipe are compared with the pressure drop formula proposed by Kandlikar [30]. The theoretical pressure drop formula is shown in equation 18. The value of $f_{app}Re$ is given by Kandlika [30]. Figure 2(b) shows that the average error between the current numerical results and the theoretical data is 8.6 %. Figure 2 shows that the numerical results agree with the theoretical methods in the literature.

Results and discussion

Figure 3 shows that in comparison the SMC, the velocity boundary-layers of the three rectangular mini-channels with different *S*-shaped turbulator are thinner. Furthermore, the maximum velocity region is distributed on both sides of the channel but is not perfectly symmetrical. The maximum velocity region appears between the *S*-shaped turbulator and the walls. It has a certain degree of periodic variation due to the influence of the *S*-shaped turbulator. A certain degree of periodic change on both sides of the channel is affected by the *S*-shaped turbulator and a phase difference of π . Among the three rectangular mini-channels with different *S*-shaped turbulators, the smaller the radius of the horizontal axis, the stronger the disturbance effect of the turbulator on the fluid and the greater the maximum velocity.

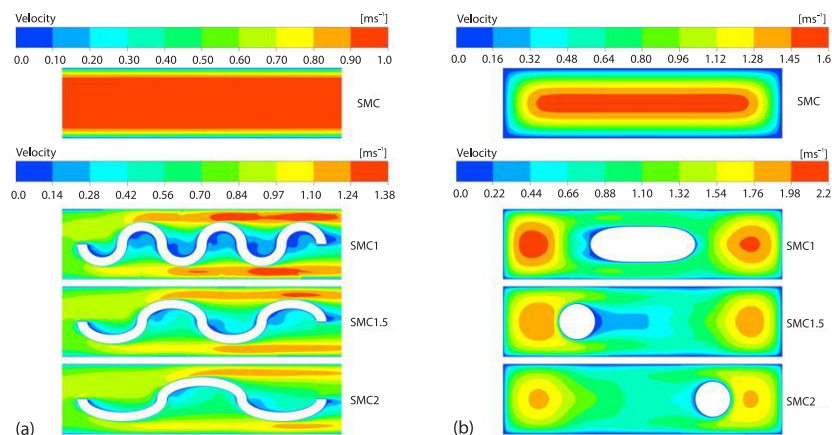


Figure 3. Velocity contours of transverse/longitudinal sections of four mini-channels; (a) velocity cloud diagram of cross-section at $y = 0$ mm ($Re = 1192.60$), and (b) velocity cloud diagram of longitudinal section at $x = 11$ mm ($Re = 1987.67$)

The cross-sectional pressure drop of three rectangular mini-channels with the *S*-shaped turbulator are faster than those in the SMC without the *S*-shaped turbulator, as shown in fig. 4. In the three rectangular mini-channels with different *S*-shaped turbulator, the smaller the transverse axis radius is, the faster the cross-sectional pressure drop. Influenced by the *S*-type turbulator, the pressure drop has a certain degree of periodic fluctuation.

It can be observed from fig. 5 that the inlet and outlet pressure drop of the three rectangular mini-channels with different *S*-shaped turbulator inserted and the SMC increase with the increase of the Reynolds number. The pressure drop of the four mini-channels with the increasing speed of the Reynolds number is $SMC1 > SMC1.5 > SMC2 > SMC$. The low the Reynolds number, the growth rate of the pressure drop of the four mini-channels is low. When the Reynolds number is high, the growth rate of the inlet and outlet pressure drop of the four mini-channels is relatively large. The rectangular mini-channel with an *S*-shaped turbulator inserted will increase the pressure drop at the inlet and outlet. The higher the Reynolds

number, the more obvious the increase in pressure drop. Compared with SMC, the pressure drop of SMC1, SMC1.5, and SMC2 are increased by 334.8-774.3%, 275.9-606.4%, and 234.6-500.4%, respectively.

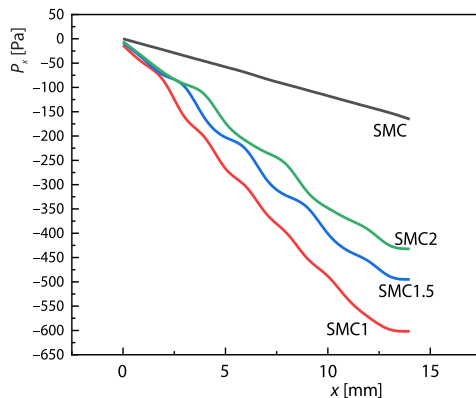


Figure 4. Cross-sectional pressure change diagram of four kinds of mini-channels along the flow direction (x), $Re = 795.07$

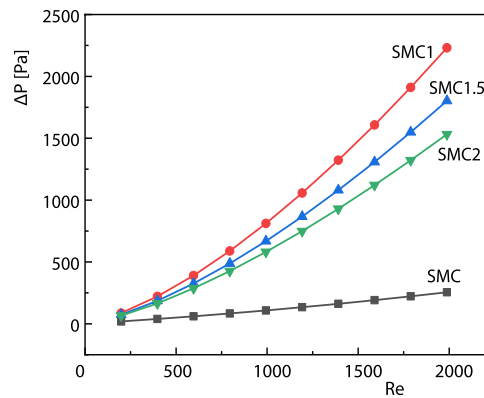


Figure 5. Variation of inlet and outlet pressure drop with Reynolds number of four mini-channels

Figure 6 shows the local Nusselt number variation of the four micro-channels at Reynolds numbers of 397.53, 795.07, 1192.60, and 1987.67, respectively. Figure 6 indicates that the local Nusselt number of the rectangular mini-channel with an *S*-shaped turbulator is higher than the SMC at the entry. The local Nusselt number of the rectangular mini-channel with an *S*-shaped turbulator displays a similar lowering tendency as the local Nusselt number of the smooth rectangular channel in a brief segment after the entrance. However, its descending gradient is more extensive and smaller than the SMC that appears locally. Unlike the SMC, the local Nusselt number of the rectangular mini-channel with an *S*-shaped turbulator quickly enters a stable state. It exhibits a steady periodic fluctuation state affected by the *S*-type turbulator. Although the local Nusselt number of the rectangular mini-channel with an *S*-shaped turbulator is in a state of regular periodic fluctuations, its local Nusselt number is higher than that of the smooth mini-channel in both peaks and valleys. Comparing the local Nusselt numbers of the three rectangular mini-channels with different *S*-shaped turbulators, $SMC1 > SMC1.5 > SMC2$. This condition can be explained in the initial stage since the turbulator has just been arranged in the channel. The head of the turbulator causes a significant local change in the fluid-flow direction. This significant change will become more severe as the Reynolds number increases and local Nusselt number drop rapidly, even slightly below the smooth mini-channel.

As shown in fig. 7, the average Nusselt number of rectangular mini-channel with an *S*-shaped turbulator is much greater than that of the smooth mini-channel. Under the same Reynolds number, the average Nusselt numbers of SMC1, SMC1.5, and SMC2 increased by 28.7-98.6%, 18.8-92%, and 11.1-88.5%, respectively, compared with SMC. The average Nusselt numbers of the smooth mini-channel and three rectangular mini-channels with different *S*-shaped turbulators all increase with the increase of Reynolds number. The growing trend is parabolic, and the rate of increase is gradually decreasing. When the Reynolds number is low, the average Nusselt number of three rectangular mini-channels with different *S*-shaped turbulators increases significantly faster than the smooth mini-channel. The comparison results of these three types are $SMC1 > SMC1.5 > SMC2$. When the Reynolds number is high, the growth rate of the average Nusselt number of the four kinds of mini-channels is significantly re-

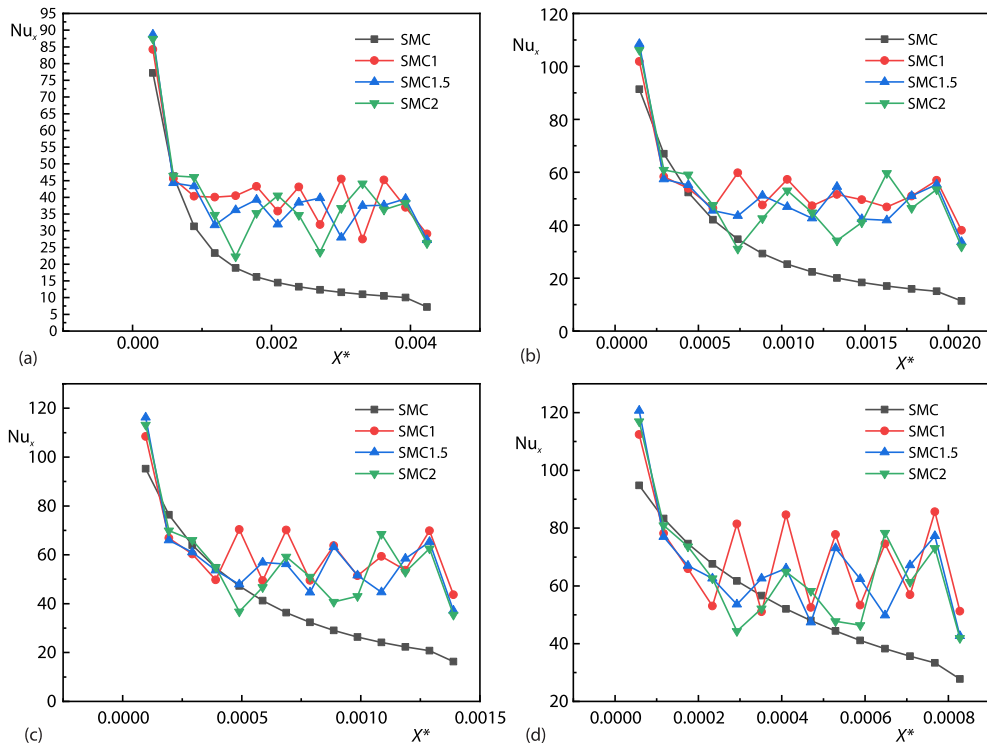


Figure 6. Variation of local Nusselt number of four mini-channels (a) $Re = 397.53, X^* = 0-0.00424$, (b) $Re = 795.07, X^* = 0-0.0021$, (c) $Re = 1192.60, X^* = 0-0.00139$, and (d) $Re = 1987.67, X^* = 0-0.00083$

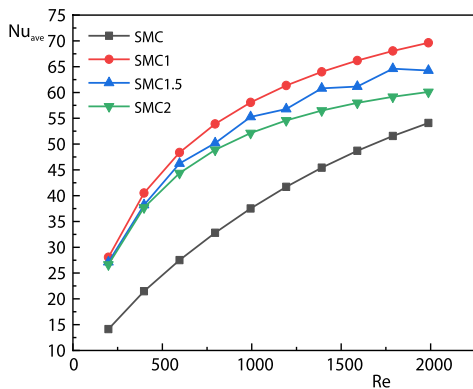


Figure 7. Variation of the average Nusselt number with Reynolds number for four mini-channels

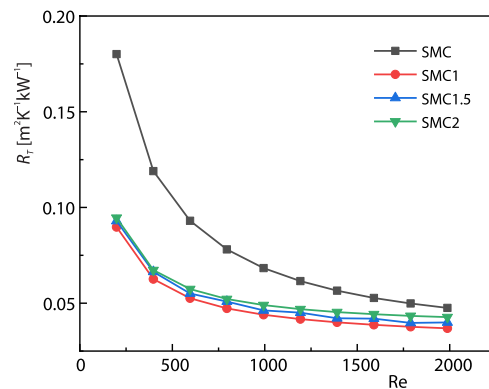


Figure 8. Relationship between total thermal resistance of four mini-channels and Reynolds number

duced. Furthermore, the rate of increase of the average Nusselt number of the three rectangular mini-channels with different S-shaped turbulators has no obvious advantage compared with the smooth mini-channels, even locally smaller than the smooth mini-channel.

Figure 8 shows the total thermal resistance vs. Reynolds number for the four mini-channels. Over the simulation range, the total thermal resistance of the four mini-channels exhibits a decreasing pattern similar to an inverse proportional function as the Reynolds number in-

creases. As the Reynolds number increases, the rate of decrease gradually decreases. When the Reynolds number is low, the thermal resistance decreases more rapidly. When the Reynolds number is high, the thermal resistance reduction rate becomes smaller, showing a trend of gradually leveling off. Compared with SMC, the total thermal resistance of SMC1, SMC1.5, and SMC2 is reduced by 22.43-50.15%, 15.91-48.40%, and 10.08-47.45%, respectively.

Figure 9 shows the variation of four kinds of mini-channel field co-ordination number, F_c , with Reynolds number. Compared with SMC in the studied Reynolds number range, the F_c of SMC1, SMC1.5 and SMC2 were increased by 30.36-115.29%, 19.72-106.94%, 19.72-104.72%, respectively. The thermal and velocity boundary-layer of the fluid in the SMC are thick. The S-shaped turbulator in the mini-channel changes the flow trajectory of the fluid and aggravates the fluid disturbance in the mini-channel. The presence of the S-shaped turbulator additionally reduces the channel's synergy angle and increases the Nusselt number, enhancing the heat transfer impact. The F_c number of SMC1 channel is higher than that of SMC1.5 and SMC2 channels. Because SMC1 has a greater turbulence effect.

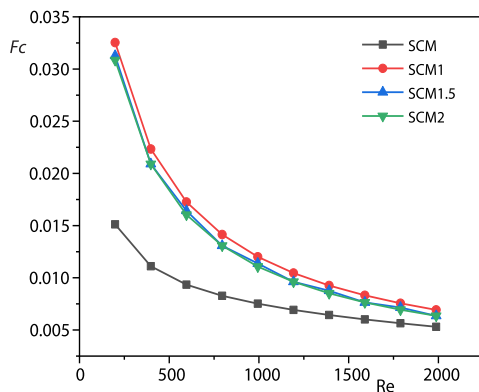


Figure 9. Variation of four kinds of mini-channel field co-ordination number, with Reynolds number

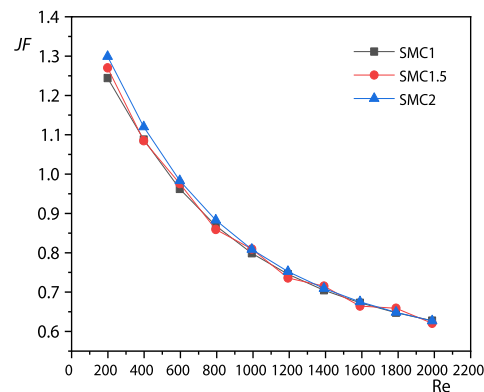


Figure 10. The variation of JF with Reynolds number

According to the aforementioned pressure drop analysis, it can be seen that the turbulator increases the Nusselt number and also increases the pressure drop. Therefore, it is necessary to comprehensively compare the heat transfer enhancement performance in these cases. In this study, the JF factor is used to evaluate the thermal hydraulic performance of the channel. The JF formula is as follows.

Friction factor:

$$f = \frac{\Delta P}{2\rho u^2} \quad (18)$$

Heat transfer factor:

$$j = \frac{Nu}{Re Pr^{1/3}} \quad (19)$$

The JF factor:

$$JF = \frac{j}{\left(\frac{f}{f_0}\right)^{1/3}} \quad (20)$$

where j_0 and f_0 are the j and f factors of the smooth channel.

Figure 10 shows the variation of JF with the Reynolds number. It can be seen that JF decreases with the increase of Reynolds number. From the changing trend of JF , the turbulator at a low Reynolds number has a better heat transfer effect on the channel.

Table 3 shows the previous research on inserts in mini-channel heat exchangers with the same geometry. At high Reynolds numbers, the effect of the turbulator may not be as good as the twisted tapes mentioned in Feng *et al.* [21]. However, at low Reynolds numbers, the ability of the turbulator to increase heat transfer efficiency is the best of the four inserts in the table.

Table 3. Comparison of different interpolators for same geometric shape channel

Authors	Inner-inserts	Fluid	Re	Nu grow
[21]	Twisted tapes	Water	419-884	29-149%
[31]	Wire coil	Water	188-1458	20-80%
[17]	LVG	Water	100-1100	2-25%
This paper	S-shaped turbulators	Water	198.77-1987.67	29-99%

Based on the simulation results, the prediction formulas of flow and heat exchange are established by the non-linear regression method. The Nu_{ave} is related to turbulator parameters (a , b) and Reynolds number and Prandtl number. Its prediction formula can be expressed:

$$Nu_{ave} = 3.708 \left(\frac{a}{b} \right)^{0.154} Re^{0.318} Pr^{1/3} \quad (21)$$

The correlation coefficient $R = 0.989$ for the Nu_{ave} prediction formula.

Usually, due to mini-channel length is short, the fluid in the rectangular mini-channel with an S-shaped turbulator is in the turbulator development region, so the pressure drop prediction formula is given in the form of the apparent friction coefficient f_{app} :

$$\Delta P = \frac{2f_{app} Re \mu_m u_{in} L_{ch}}{D_h^2} \quad (22)$$

The simulation results establish a prediction formula for the product of the Reynolds number and apparent friction coefficient. Over the length L_c from the inlet, the prediction formula in a channel with a hydraulic diameter D_h can be expressed:

$$f_{app} Re = mx^{+n} \quad (23)$$

Table 4 shows the values of m and n . The correlation coefficients of the three channels voltage drop prediction formulas for SMC1, SMC1.5, and SMC2 are $R = 0.997$, $R = 0.998$, and $R = 0.999$, respectively.

Table 4. Prediction formula dimensionless coefficient table for the product of Reynolds number and apparent friction coefficient

Mini-channel	m	n
SMC1	25.134	-0.425
SMC1.5	23.134	-0.401
SMC2	22.598	-0.376

Figures 11 and 12 are the comparison of predicted formula values and simulated values. When $Re = 198.76$, the variances between Nu_{ave} projected values and simulated SMC1, SMC1.5, and SMC2 are 15.62%, 12.56%, and 9.45%, respectively, as shown in fig. 9(a). Fur-

thermore, the Nu_{ave} predicted and simulated values for different Reynolds numbers are within $\pm 4.6\%$ of each other. It can be seen from fig. 10 that when $Re = 198.76$, the deviations of the predicted pressure drop and the simulated value of the three mini-channels of SMC1, SMC1.5, and SMC2 are 22.32%, 21.17%, and 19.97%, respectively. In addition, the deviations between the predicted and simulated pressure drop values at other Reynolds numbers are all within $\pm 14\%$.

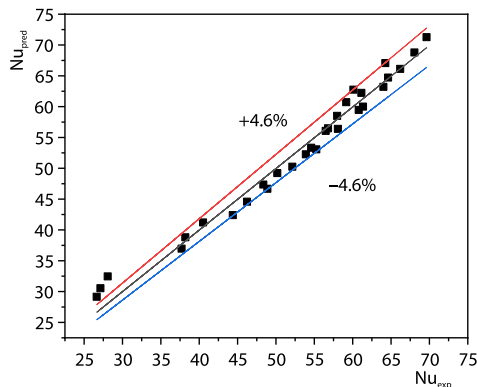


Figure 11. Comparison of predicted and simulated average Nusselt number

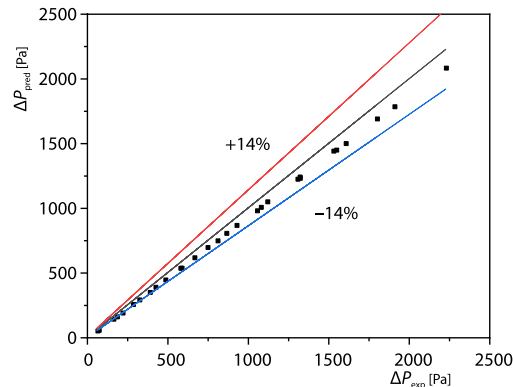


Figure 12. Comparison of predicted and simulated pressure drop

Conclusion

In this paper, the fluid's heat transfer characteristics and flow in the SMC and three rectangular mini-channels with different horizontal axis radii S -shaped turbulators are studied by numerical simulation under constant wall temperature heating in the range of Reynolds number 198.77~1987.67. The rectangular mini-channel with an S -shaped turbulator has a higher pressure drop, a higher average Nusselt number, a lower overall thermal resistance and a higher field coordination number than the smooth mini-channel. For SMC1, SMC1.5, and SMC2, the pressure drop in these three mini-channels increased by 334.8-774.3%, 275.9-606.4%, and 234.6-500.4%, respectively. The average Nusselt number increased by 28.7-98.6%, 18.8-92%, and 11.1-88.5%, respectively. The total thermal resistance was reduced by 22.43-50.15%, 15.91-48.40%, and 10.08-47.45%, respectively. The Fc increased by 30.36-115.29%, 19.72%-106.94% and 19.72-104.72%, respectively. It is found that the smaller the horizontal axis radius, The larger the pressure drop, the smaller the total thermal resistance, the higher the average Nusselt number and the larger the field coordination number. The prediction formulas for the average Nusselt number and pressure drop are developed using the non-linear regression approach based on the simulated data. In most situations, the differences between the predicted and simulated values are less than 4.6% and 14%, respectively.

Nomenclature

A – heating surface area, [m²]
 A_c – cross-sectional area, [m²]
 a – horizontal axis radius, [mm]
 b – vertical axis radius, [mm]
 c – distances between the S -shaped turbulator and the channel wall, [mm]
 $c_{p,f}$ – specific heat at constant pressure, [kJkg⁻¹k⁻¹]
 d – distances between the S -shaped turbulator and the channel wall, [mm]

D_h – hydraulic diameter, [mm]
 ΔP – pressure drop, [Pa]
 f – friction factor
 Fc – field co-ordination number
 H – height of computational domain, [mm]
 h_{ave} – average convective heat transfer coefficient, [Wm⁻²K⁻¹]
 h_x – local convective heat transfer coefficient,
 j – heat transfer factor

JF – thermal performance factor
 L_a – length of the inlet section, [mm]
 L_b – length of the heating section, [mm]
 L_c – length of the outlet section, [mm]
 L_{ch} – channel length
 m – dimensionless coefficient
 n – dimensionless coefficient
 Nu_{ave} – average Nusselt number
 Nu_x – local Nusselt number
 P_{in} – inlet pressure, [Pa]
 P_{out} – outlet pressure, [Pa]
 Pr – Prandtl number
 Q – heat transfer rate, [W]
 Re – Reynolds number
 R_T – total thermal resistance, [$m^2K^{-1}W^{-1}$]
 r – turbulator radius, [mm]
 T_{in} – inlet temperature, [K]
 T_{out} – outlet temperature, [K]
 T_{wall} – wall temperature, [K]
 u_{in} – inlet velocity, [ms^{-1}]

W – width, [mm]
 X^* – dimensionless distance

Greek symbols

α – synergy angle between the fluid velocity vector and the temperature gradient, [$^\circ$]
 β – synergy angle between the fluid velocity vector and the pressure gradient, [$^\circ$]
 μ – viscosity, [Pa·s]
 ρ – density, [kgm^{-3}]
 λ – thermal conductivity, [$Wm^{-1}K^{-1}$]

Subscripts

ave – average
 f – fluid
 in – inlet
 out – outlet
 wall – solid wall
 x – local

Acknowledgment

This paper was supported by the Innovative Research Team of Henan Polytechnic University (T2020-3).

References

- [1] Tuckerman, D., Pease, R. F. W., High-Performance Heat Sinking for VLSI, *Electron Device Letters, IEEE*, 2 (1981), 5, pp. 126-129
- [2] Lelea, D., *et al.*, The Experimental Research on Microtube Heat Transfer and Fluid-Flow of Distilled Water, *International Journal of Heat and Mass Transfer*, 47 (2004), 12, pp. 2817-2830
- [3] Shah, R. K., London, A. L., *Laminar Flow Forced Convection in Ducts: A Source Book for Compact Heat Exchanger Analytical Data*, Academic Press, New York, USA, 1978, pp. 78-138
- [4] Blevins, R., *Applied Fluid Dynamics Handbook*, Van Nostrand Reinhold Company, New York, USA, 1984
- [5] Bezaatpour, M., Goharkhah, M., Convective Heat Transfer Enhancement in a Double Pipe Mini Heat Exchanger by Magnetic Field Induced Swirling Flow, *Applied Thermal Engineering*, 167 (2020), 114801
- [6] Hajmohammadi, M. R., *et al.*, Effects of Applying Uniform and Non-Uniform External Magnetic Fields on the Optimal Design of micro-channel heat sinks, *International Journal of Mechanical Sciences*, 186 (2020), 105886
- [7] Krishan, G., *et al.*, Synthetic Jet Impingement Heat Transfer Enhancement – A Review, *Applied Thermal Engineering*, 149 (2019), Feb., pp. 1305-1323
- [8] Yu, F., *et al.*, Experimental Investigation of Flow Boiling Heat Transfer Enhancement under Ultrasound Fields in a Minichannel Heat Sink, *Ultrasonics Sonochemistry*, 70 (2021), 105342
- [9] Zhou, J., *et al.*, Flow Boiling Heat Transfer Enhancement under Ultrasound Field in Minichannel Heat Sinks, *Ultrasonics Sonochemistry*, 78 (2021), 105737
- [10] Robinson, A. J., *et al.*, A Single Phase Hybrid Micro Heat Sink Using Impinging Micro-Jet Arrays and Micro-Channels, *Applied Thermal Engineering*, 136 (2018), May, pp. 408-418
- [11] Liang, G., Mudawar, I., Review of Single-Phase and Two-Phase Nanofluid Heat Transfer in Macro-Channels and Micro-Channels, *International Journal of Heat and Mass Transfer*, 136 (2019), June, pp. 324-354
- [12] Qu, W., Mudawar, I., Experimental and Numerical Study of Pressure Drop and Heat Transfer in a Single-Phase Micro-Channel Heat Sink, *International Journal of Heat and Mass Transfer*, 45 (2002), 12, pp. 2549-2565
- [13] Tian, L., *et al.*, Numerical Study of Fluid-Flow and Heat Transfer in a Flat-Plate Channel with Longitudinal Vortex Generators by Applying Field Synergy Principle Analysis, *International Communications in Heat and Mass Transfer*, 36 (2009), 2, pp. 111-120

- [14] Sohankar, A., Heat Transfer Augmentation in a Rectangular Channel with a Vee-Shaped Vortex Generator, *International Journal of Heat and Fluid-Flow*, 28 (2007), 2, pp. 306-317
- [15] Wang, Y., et al., Numerical Study and Performance Analyses of the Mini-Channel with Discrete Double-Inclined Ribs, *International Journal of Heat and Mass Transfer*, 78 (2014), Nov., pp. 498-505
- [16] Fiebig, M., Embedded Vortices in Internal Flow: Heat Transfer and Pressure Loss Enhancement, *International Journal of Heat and Fluid-Flow*, 16 (1995), 5, pp. 376-388
- [17] Ebrahimi, A., et al., Numerical Study of Liquid-Flow and Heat Transfer in Rectangular Micro-Channel with Longitudinal Vortex Generators, *Applied Thermal Engineering*, 78 (2015), Mar., pp. 576-583
- [18] Datta, A., et al., Numerical Investigation of Heat Transfer in Micro-Channel Using Inclined Longitudinal Vortex Generator, *Applied Thermal Engineering*, 108 (2016), Sept., pp. 1008-1019
- [19] Yadav, V., et al., Numerical Investigation of Heat Transfer in Extended Surface Micro-Channels, *International Journal of Heat and Mass Transfer*, 93 (2016), Feb., pp. 612-622
- [20] Jia, Y., et al., Heat Transfer and Fluid-Flow Characteristics of Combined Micro-Channel with Cone-shaped micro pin fins, *International Communications in Heat and Mass Transfer*, 92 (2018), Mar., pp. 78-89
- [21] Feng, Z., et al., Experimental Investigation of Laminar Flow and Heat Transfer Characteristics in Square Minichannels with Twisted Tapes, *International Journal of Heat and Mass Transfer*, 158 (2020), 119947
- [22] Kurnia, J. C., et al., Laminar Convective Heat Transfer in Helical Tube with Twisted Tape Insert, *International Journal of Heat and Mass Transfer*, 150 (2020), 119309
- [23] Saysroy, A., Eiamsard, S., Periodically Fully-Developed Heat and Fluid-Flow Behaviors in a Turbulent Tube Flow with Square-Cut Twisted Tape Inserts, *Applied Thermal Engineering*, 112 (2017), Feb., pp. 895-910
- [24] Zheng, S., et al., Numerical Investigation on Thermal-Hydraulic Characteristics in a Mini-Channel with Trapezoidal Cross-Section Longitudinal Vortex Generators, *Applied Thermal Engineering*, 205 (2022), 118004
- [25] Ebrahimi, A., Naranjani, B., An Investigation on Thermo-Hydraulic Performance of a Flat-Plate Channel with Pyramidal Protrusions, *Applied Thermal Engineering*, 106 (2016), Aug., pp. 316-324
- [26] Ebrahimi, A., et al., Laminar Convective Heat Transfer of Shear-Thinning Liquids in Rectangular Channels with Longitudinal Vortex Generators, *Chemical Engineering Science*, 173 (2017), Dec., pp. 264-274
- [27] Sui, Y., et al., An Experimental Study of Flow Friction and Heat Transfer in Wavy Micro-Channels with Rectangular Cross-Section, *International Journal of Thermal Sciences*, 50 (2011), 12, pp. 2473-2482
- [28] Zhu, Q., et al., Effects of Geometric Parameters on Fluid-Flow and Heat Transfer in Micro-Channel Heat Sink with Trapezoidal Grooves in Sidewalls, *Thermal Science*, 26 (2022), 4B, pp. 3641-3651
- [29] Lin, Z., et al., Heat Transfer Augmentation Characteristics of a Fin Punched with Curve Trapezoidal Vortex Generators at the Rear of Tubes, *Thermal Science*, 26 (2022), 4B, pp. 3529-3544
- [30] Kandlikar, S. G., Single-Phase Liquid-Flow in Minichannels and Micro-Channels, in: *Heat Transfer and Fluid-flow in Minichannels and Micro-Channels* (Eds. Kandlikar, S. G., et al.), Elsevier Science Ltd., Oxford, UK, 2006, Chapter 3, pp. 87-136
- [31] Feng, Z., et al., Numerical Investigation on Laminar Flow and Heat Transfer in Rectangular Micro-Channel Heat Sink with Wire Coil Inserts, *Applied Thermal Engineering*, 116 (2017), Apr., pp. 597-609